ACS APPLIED MATERIALS & INTERFACES

Research Article

Cite This: ACS Appl. Mater. Interfaces 2018, 10, 20621−20626

www.acsami.org

Ab Initio Metadynamics Study of the VO_2^+/VO^{2+} Redox Reaction Mechanism at the Graphite Edge/Water Interface

Zhen Jiang,[†] Konstantin Klyukin,[†] and Vitaly Alexandrov*[,†,‡]

[†]Department of Chemical and Biomolecular Engineering and [‡]Nebraska Center for Materials and Nanoscience, University of Nebraska−Lincoln, Lincoln, Nebraska 68588, United States

Supporting Information

ABSTRACT: Redox flow batteries (RFBs) are promising electrochemical energy storage systems, for which development is impeded by a poor understanding of redox reactions occurring at electrode/electrolyte interfaces. Even for the conventional all-vanadium RFB chemistry employing V^{2+}/V^{3+} and VO_2^+/VO^{2+} couples, there is still no consensus about the reaction mechanism, electrode active sites, and rate-determining step. Herein, we perform Car−Parrinello molecular dynamics-based metadynamics simulations to unravel the mechanism of the VO_2^+/VO^{2+} redox reaction in water at the oxygen-functionalized graphite $(11\bar{2}0)$ edge surface serving as a representative carbon-based electrode. Our results suggest that during the battery discharge aqueous VO_2^+/VO^{2+} species adsorb at the surface C−O groups as inner-sphere complexes, exhibiting faster adsorption/desorption kinetics than V^{2+}/V^{3+}, at least at low vanadium concentrations considered in our study. We find that this is because (i) VO_2^+/VO^{2+} conversion does not involve the slow transfer of an oxygen atom, (ii) protonation of VO_2^+ is spontaneous and coupled to interfacial electron transfer in acidic conditions to enable VO^{2+} formation, and (iii) V^{3+} found to be strongly bound to oxygen groups of the graphite surface features unfavorable desorption kinetics. In contrast, the reverse process taking place upon charging is expected to be more sluggish for the VO_2^+/VO^{2+} redox couple because of both unfavorable deprotonation of the VO^{2+} water ligands and adsorption/desorption kinetics.

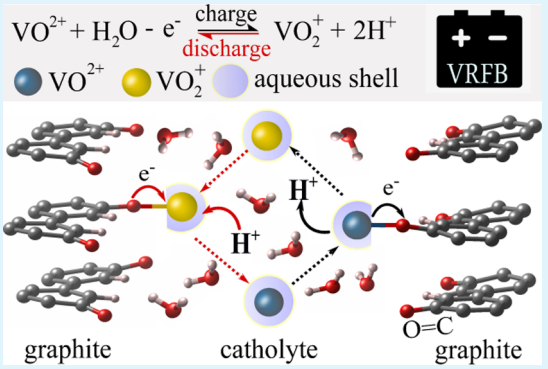

KEYWORDS: *vanadium redox flow batteries, ab initio molecular dynamics, reaction mechanism, graphite, oxygen-functional groups*

1. INTRODUCTION

Redox flow batteries (RFBs) represent viable electrochemical energy storage systems that have been recently gaining a great deal of attention for grid-scale applications.[1−7] RFBs offer a number of advantages such as flexible design because of the decoupling of energy and power density, the absence of phase transformations typical for solid-state batteries, high energy efficiency, and long-term storage of charge. While various RFB chemistries were proposed in the past, poor understanding of elementary electrochemical processes occurring in both aqueous electrolytes and at electrode surfaces still hampers the practical utilization of most RFBs. The all-vanadium redox flow battery (VRFB) is among the most well-studied RFBs.[8−14] In a completely charged state, the VRFB catholyte is comprised of only VO_2^+ and the anolyte is comprised of only V^{2+} redox species dissolved in a sulfuric acid-based aqueous solution. Upon battery cycling, the cell undergoes the following redox reactions:

$$VO_2^+ + 2H^+ + e^- \underset{\text{charge}}{\overset{\text{discharge}}{\rightleftharpoons}} VO^{2+} + H_2O,\ E^0 = 1\ \text{V vs RHE}$$

in the positive half-cell and

$$V^{2+} \underset{\text{charge}}{\overset{\text{discharge}}{\rightleftharpoons}} V^{3+} + e^-,\ E^0 = -0.26\ \text{V vs RHE}$$

in the negative half-cell.

The power density of RFBs is primarily determined by the kinetics of redox reactions occurring at electrolyte/electrode interfaces and is strongly dependent on the surface chemistry of electrode materials. Pristine carbon materials such as graphite are commonly used as RFB electrodes, but they suffer from low electrochemical activity and poor reversibility.[11,13,14] To improve the electrode performance, various surface functionalization strategies have been proposed including thermal activation, chemical oxidation, surface doping, and decoration by nanoparticles.[14−18] Carbon surface modification through the introduction of oxygen functional groups such as OH, COH, and COOH has been found as a particularly efficient way to accelerate interfacial redox reaction kinetics by several orders of magnitude.[13,19,20] However, this enhancement in electrochemical activity of carbon materials depends strongly on the

Received: April 12, 2018
Accepted: May 29, 2018
Published: May 29, 2018

DOI: 10.1021/acsami.8b05864
ACS Appl. Mater. Interfaces 2018, 10, 20621−20626

amount and nature of oxygen functional groups at electrode surfaces, electrode nature (graphite, graphene, carbon nanotubes), and surface structure (basal, edge).[19,21,22] It also depends on the concentration of redox active species dissolved in the electrolyte.[21] Because of the complexity of the phenomenon, there is still no consensus about atomistic details on the redox reaction mechanism even for the conventional VRFBs as it is challenging to experimentally deconvolute various contributions to the redox reaction kinetics [mass and electron transfer (ET)], identify the main active surface sites, and determine the rate-determining step of the overall redox process.

In the past, multiple mechanisms were proposed for the VO_2^+/VO^{2+} and V^{2+}/V^{3+} reactions based on experimental data. These include redox reactions proceeding via outer-sphere species, as well as inner-sphere mono- and bidentate vanadium complexes adsorbed at carbon electrode surfaces.[13,19,23] It was experimentally determined that vanadium ions have a low propensity for adsorption on pristine carbon surfaces, whereas surface oxygen groups increase the wetted surface area[19] and should act as active sites for both adsorption of vanadium ions and accelerated interfacial ET.[24]

Overall, it has been a conventional belief that it is the VO_2^+/VO^{2+} redox reaction, not V^{2+}/V^{3+}, that should be rate limiting as it involves the transfer of both an electron and an oxygen atom. Experimental kinetics data, however, are highly scattered and even the measured ET rate constants demonstrate that either of the two half-cell reactions can exhibit slower kinetics depending on multiple factors.[19]

As for the specific role of surface oxygen groups on carbon electrodes, some studies revealed that their presence can in fact impede the VO_2^+/VO^{2+} redox reaction.[19,25] It was demonstrated that the rate constants for the V^{2+}/V^{3+} redox reaction increase and for the VO_2^+/VO^{2+} reaction decrease with increasing amount of OH, COH, and COOH groups at graphite surfaces. Thus, the trends for the two half-cell reactions were observed to be diametrical. It was hypothesized, by analogy with the $[Fe(CN)_6]^{4-}/[Fe(CN)_6]^{3-}$ system where iron oxide precipitation was also observed, that the VO_2^+/VO^{2+} reaction kinetics could be impeded relative to pristine graphite because of the formation of VO_x passivating layers on graphite. In contrast, surface oxygen groups catalyze V^{2+}/V^{3+} conversion via the formation of inner-sphere complexes between adsorbed vanadium and surface oxygen ions.

The observed scattering in redox kinetics data for VRFBs is in large part due to experimental complications in controlling the composition of electrode materials and detecting reaction rate constants at the nanoscale. In this regard, atomistic first-principles simulations provide a way to model reaction mechanisms under well-defined conditions and investigate chemical characteristics of individual reaction sites and reaction environment. Moreover, ab initio molecular dynamics (AIMD) methods allow one to capture the dynamic nature of the process explicitly, including solvent and entropy effects. In this study, by employing a series of AIMD simulations we investigate the VO_2^+/VO^{2+} reaction mechanism at the graphite $(11\bar{2}0)$ edge surface as a representative carbon-based electrode material used in VRFBs.

2. COMPUTATIONAL DETAILS

Simulations were performed utilizing a 12.70 × 13.54 × 14.90 Å box comprised of the graphite slab and a vacuum gap of 10 Å with a vanadium ion (V^{2+}, V^{3+}, VO^{2+}, VO_2^+) embedded into solution of 53 H_2O molecules to obtain the water density of approximately 1 g/cm^3 (Figure 1). The graphite edge $(11\bar{2}0)$ surface was functionalized by C═O groups serving as reaction sites as the result of complete water dissociation according to previous computational results.[24] The concentration of these functional groups at carbon edges was experimentally observed to increase for the heat-treated carbon which was hypothesized to be the reason for the enhanced redox kinetics relative to the as-received carbon with a lower content of surface oxygen functional groups.[13,19,21,22] To ensure charge neutrality of the simulation cell, one/two protons from the opposite side of the graphite slab were removed resulting in the formation of epoxyl group(s) on the surface.

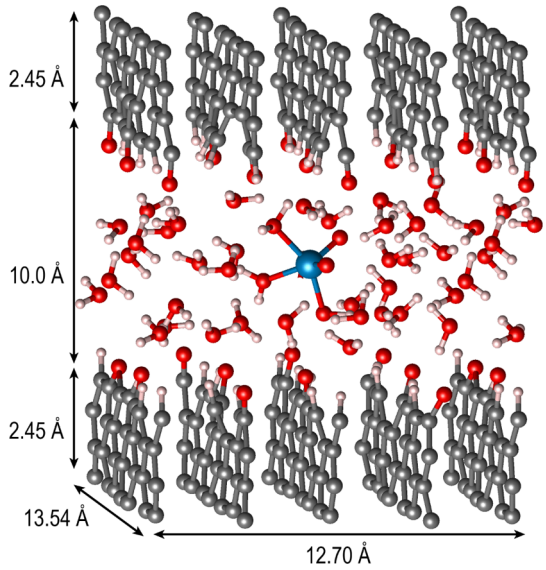

Figure 1. Simulation cell used to model the redox reaction mechanism for the aqueous VO^{2+}/VO_2^+ couple.

All calculations were carried out within the plane-wave density-functional-theory (DFT) framework as implemented in the NWChem code.[26] The exchange and correlation energies were calculated using the Perdew–Burke–Ernzerhof (PBE) functional within the generalized gradient approximation.[27] The PBE functional was corrected for van der Waals interactions using the Grimme approach (PBE-D3 with BJ damping).[28] The norm-conserving Troullier–Martins pseudopotentials[29] were applied for vanadium, whereas Hamann pseudopotentials[30,31] were used for oxygen, carbon and hydrogen. The kinetic cutoff energies of 60 and 120 Ry were applied to expand the Kohn–Sham electronic wave functions and charge density, respectively. V^{2+}, V^{3+} and VO^{2+} species were considered within a spin-unrestricted formalism. To interpret oxidation states of the vanadium species, Bader charge analysis was performed based on static DFT calculations. Similar DFT methodologies were previously employed to study structural properties of vanadium ions in aqueous solutions[32,33] and their interactions with graphite surfaces[24] and membranes.[34,35]

Free-energy simulations were performed utilizing Car–Parrinello molecular dynamics (CPMD) simulations[36] in combination with direct metadynamics[37,38] to accelerate sampling of free-energy landscapes associated with vanadium redox reactions in aqueous environments at room temperature. This approach has proved to be very successful in simulating rare events and estimating activation free-energy barriers for a

DOI: 10.1021/acsami.8b05864
ACS Appl. Mater. Interfaces 2018, 10, 20621–20626

variety of chemical processes.[38−42] To maintain the system temperature at 300 K, the Nosé−Hoover thermostat[43,44] was employed. Each system was initially pre-equilibrated using a QM/MM potential[45] during 6 ps, followed by additional CPMD equilibration for at least 6 ps. Hydrogen atoms were replaced with deuterium to facilitate numerical integration. A fictitious electronic mass of 600 au and a simulation time step of δt = 5 au (0.121 fs) were set. Configurations from the post-equilibration CPMD simulations used for further analysis were saved at time intervals of 10δt. The CPMD-based metadynamics approach[37,38] was employed to accelerate free-energy landscape sampling and compute activation barriers using CPMD equilibrated systems. The height and width of repulsive Gaussian hills were set to 0.001 au (0.63 kcal/mol) and 0.1 au, respectively, and were added to the potential every 100δt. The Gaussian height was chosen to be small enough to provide accurate estimation of activation barriers based on several test simulations and our previous investigation of V^{2+}/V^{3+} adsorption/desorption kinetics.[24] In total, a CPMD trajectory of about 550 ps long was analyzed in our study.

The bond distance between an adsorbing/desorbing vanadium cation and the oxygen atom of the graphite surface was used as the collective variable (CV). To describe the energetics of VO^{2+}/VO_2^+ protonation/deprotonation reactions at the graphite/water interfaces, an additional proton was added to the solution and the coordination number of an oxygen atom bound to the V center with respect to the number of protons attached to it was employed. In this case, k was set to 10 $Å^{-1}$ as an arbitrary positive constant, and r_{cut} was set to 1.38 Å as the standard O−H cutoff distance.

3. RESULTS AND DISCUSSION

We start by discussing the discharge reaction in which VO_2^+ is reduced to VO^{2+} in the catholyte. Figure 2 schematically shows

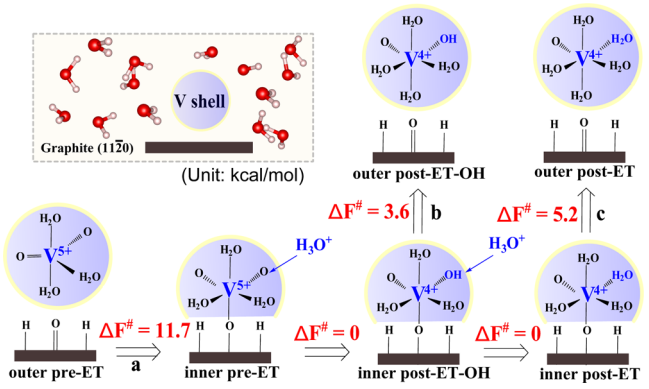

Figure 2. Schematic showing the identified mechanism of the $VO_2^+ \rightarrow VO^{2+}$ redox reaction at the graphite edge surface in aqueous solution and associated free-energy barriers (in kcal/mol) calculated by CPMD-based metadynamics. Pre- and post-ET stand for VO_2^+ species before ET and for VO^{2+} after ET has occurred, respectively.

the simulated redox reaction mechanism along with the free energy barriers for all reaction steps as estimated from CPMD-based metadynamics simulations. The first step is the adsorption of aqueous VO_2^+ at the graphite edge C═O site starting from the outer-sphere complex and transforming into the inner-sphere adsorption configuration (step **a**). During this step, characterized by a free energy barrier of 11.7 kcal/mol, the V^{5+} cation of aqueous VO_2^+ changes its coordination from five- to six-fold by forming an additional bond with the surface oxygen atom. This complex is found to be stable in CPMD simulations at room temperature in the adsorbed state.

Because aqueous electrolytes employed in VRFBs are characterized by acidic pH, we next consider the effect of an extra proton in solution charge-compensated by the removal of one H^+ from the other side of the graphite edge surface. Both CPMD and static DFT calculations reveal that if an extra H_3O^+ ion is placed in the vicinity of the adsorbed VO_2^+ ion, the vanadium ion gets spontaneously protonated. This is found to be accompanied by interfacial ET from the graphite surface to form the inner-sphere post-ET configuration at the surface, as indicated by Bader charge analysis (Table 1). On the basis of the analysis of both ionic charges and magnetic moments, it is clearly seen that pre-ET complexes can be associated with VO_2^+, while post-ET complexes with VO^{2+} species.

When desorbed from the surface to yield an outer-sphere post-ET configuration with one OH ligand (step **b**), the positive charge on the vanadium ion with its first coordination shell increases, while the charge on vanadium stays the same as for the inner-sphere post-ET complex indicative of the V^{4+} oxidation state. If this complex attaches the second proton from solution forming additional H_2O ligands, either in inner- or outer-sphere configuration, the positive charge on vanadium ion is further increased to approach the formal +2 charge as in VO^{2+}. The interpretation of vanadium oxidation states is even more apparent from the analysis of magnetic moments that are found to be practically 0 for all pre-ET complexes (V^{5+} species) and about 1.3 μ_B for the post-ET complexes (V^{4+} species). The observed greater sensitivity of magnetic moments than ionic charges to the ET process appears to be in agreement with other computational studies.[46,47] The bond distances between the adsorbed vanadium and surface oxygen ions are also in agreement with the assigned oxidation states being about 1.99 Å for V^{5+}−O versus 2.14 Å for V^{4+}−O based on the CPMD trajectories.

The observed charge distributions qualitatively agree with the estimated free energy barriers of the desorption process for the two inner-sphere post-ET complexes. Specifically, less positively charged VO^{2+} with an OH ligand (inner post-ET-OH complex) features a slightly lower desorption barrier (~3.6 kcal/mol) because of a weaker electrostatic attraction to the surface oxygen group than the complex with an H_2O ligand (inner post-ET) characterized by a ~5.2 kcal/mol desorption barrier. It should be noted that given the values of the free energy barrier and error estimated for the VO^{2+} complex with an OH ligand (3.6 ± 1.5 kcal/mol, see discussion below), its desorption is expected to be spontaneous at elevated temperatures, while the second proton can be subsequently gained upon desorption to the electrolyte solution. Overall, our simulations demonstrate that the VO^{2+}/VO_2^+ adsorption/desorption kinetics should be significantly faster than that of V^{2+}/V^{3+} during the battery discharge.[24]

We next analyze the mechanism of the reverse reaction when VO^{2+} is oxidized to VO_2^+ during the VRFB charging process. Figure 3 shows a schematic summarizing our ab initio metadynamics results for the examined interfacial process. The conversion of VO^{2+} from the outer- to inner-sphere adsorption configuration is determined to yield an activation barrier of about 14.6 kcal/mol (step **a**). This is about 3 kcal/mol larger than the adsorption energy computed for VO_2^+, in agreement with electrostatic considerations. The next reactions (steps **b** and **c**) involve two subsequent deprotonation reactions

DOI: 10.1021/acsami.8b05864
ACS Appl. Mater. Interfaces 2018, 10, 20621−20626

Table 1. Bader Charges *q*, Magnetic Moments *m*, and Interpreted Vanadium Oxidation States for Reaction Intermediates in the $VO_2^+ \rightarrow VO^{2+}$ Redox Reaction Pathway Shown in Figure 2[a]

	outer pre-ET	inner pre-ET	inner post-ET-OH	outer post-ET-OH	inner post-ET	outer post-ET
q(V shell), e	0.81	0.77	0.88	0.97	1.50	1.72
q(V), e	2.39	2.39	2.28	2.28	2.27	2.28
m(V), μ_B	0.0	0.0	1.05	1.23	1.28	1.32
oxidation state (V)	+5	+5	+4	+4	+4	+4

[a] q(V shell) stands for the charge on a vanadium cation including species from its first coordination sphere.

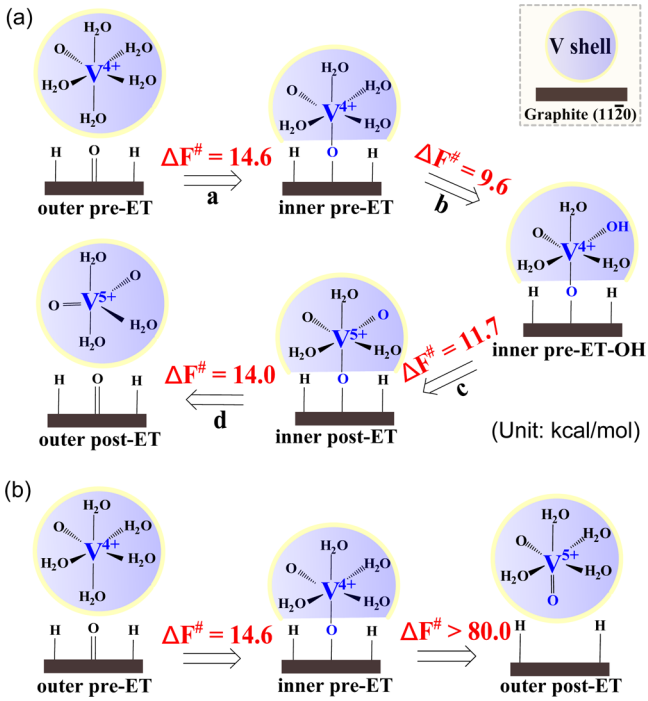

Figure 3. Schematic showing two mechanisms (a,b) of the $VO^{2+} \rightarrow VO_2^+$ redox reaction at the graphite edge surface in aqueous solution and associated free-energy barriers (in kcal/mol) calculated by CPMD-based metadynamics. Pre- and post-ET stand for VO^{2+} species before ET and for VO_2^+ after ET has occurred, respectively.

of an H_2O ligand of the VO^{2+} ion characterized by 9.6 and 11.7 kcal/mol free-energy barriers to produce VO_2^+ followed by its desorption from the inner-sphere adsorption state into solution estimated at 14 kcal/mol (step **d**). It is thus found that the process is energy-intensive, driven by application of an external voltage during the VRFB charging.

Similarly to the discharge reaction discussed earlier, our analysis of both Bader charges and magnetic moments on vanadium ions allows us to identify vanadium oxidation states and the coupling between proton and ET processes at the interface. It is seen from Table 2 that the calculated Bader charges and magnetic moments on the vanadium cations, as well as ionic charges on aqueous VO_2^+ and VO^{2+} species are all consistent with the values obtained for the discharge reaction pathway (Table 1). Also, the bond distances between the vanadium ion and oxygen atom of the surface C−O group in both pre- and post-ET inner-sphere adsorption configurations are very similar to the discharge reaction being on average 2.14 Å for V^{4+}−O and 1.99 Å for V^{5+}−O from CPMD simulations.

In addition to the mechanism of the redox reaction proceeding via inner-sphere monodentate adsorption complexes, several other mechanisms were previously put forward in the literature. For example, the reaction pathway depicted in

Table 2. Bader Charges *q*, Magnetic Moments *m*, and Interpreted Vanadium Oxidation States for Reaction Intermediates in the $VO_2^+ \rightarrow VO^{2+}$ Redox Reaction Pathway Shown in Figure 3a[a]

	outer pre-ET	inner pre-ET	inner pre-ET-OH	inner post-ET	outer post-ET
q(V shell), e	1.75	1.63	0.98	0.70	0.79
q(V), e	2.28	2.27	2.28	2.40	2.38
m(V), μ_B	1.32	1.29	1.28	0.0	0.0
oxidation state (V)	+4	+4	+4	+5	+5

[a] q(V shell) stands for the charge on a vanadium cation including species from its first coordination sphere.

Figure 3b involves detachment of a surface oxygen species from the graphite edge. The participation of a surface oxygen ion in the overall reaction mechanism was proposed experimentally[13] as a way to supply oxygen species to the adsorbed VO^{2+} ions to form VO_2^+. Quite expectedly, however, our simulations show that the system in this case needs to overcome a high activation barrier of more than 80 kcal/mol attributed to breaking a very strong surface C−O bond. Another previously hypothesized mechanism involves adsorption of VO^{2+} as a bidentate complex with V^{4+} forming covalent bonds with two surface oxygen atoms.[13] Adsorption in this configuration is supposed to facilitate interfacial ET through two V−O bonds as compared to the monodentate case. On the other hand, desorption of the redox reaction product from this adsorption state would require a larger activation energy necessary to break two bonds after ET has occurred. To test the possibility of this reaction pathway, we have also estimated the energetics of VO^{2+} adsorption onto two C═O surface groups and found this to be larger than 40 kcal/mol. Given that the desorption energy is expected to be high as well for the post-ET state because of stronger attraction of the formed V^{5+} ion to surface oxygen atoms, the redox reaction through the bidentate adsorption configuration appears to be kinetically unfavorable. We should also comment on the role of outer-sphere adsorption complexes by noting that their involvement into the overall redox reaction should be limited by presumably slow interfacial ET because of the absence of covalent C−O−V bonds catalyzing charge transfer for both vanadium redox couples.

An important aspect of any molecular dynamics simulation is to analyze the errors associated with estimated free energies. In relation to ab initio metadynamics simulations employed in this study, a few metadynamics parameters such as the Gaussian width, height, and deposition time used to reconstruct free energies in CV space are at play. Here, the intrinsic error of the metadynamics approach associated with the activation energy barriers was assessed with the equation derived by Laio et al.,[37,38] assuming that the calculation does not depend on the starting structure and on the particular sequence of visited

DOI: 10.1021/acsami.8b05864
ACS Appl. Mater. Interfaces 2018, 10, 20621−20626

configurations. The equation was simplified for a one-dimensional CV space as shown below

$$\langle \varepsilon^2 \rangle = \sqrt{\frac{2}{\pi^3}} \frac{k_B T S h_0 w}{D \tau_g} \exp\left(-\frac{\pi^2 w^2}{2S^2}\right)$$

The error bars were calculated based on the evaluation of single trajectory parameters, which allowed to avoid extremely time-consuming calculations of statistical error by averaging several metadynamics trajectories. The error value was determined by the optimal choice of computational parameters: Gaussian hill height h_0, width w, and deposition time τ_g and by intrinsic properties of the considered system: size of the free energy well S, temperature T, and diffusion coefficient D. The computation parameters are described in the Computational Details section, and the estimation of diffusion coefficient D was obtained using the time evolution of the mean squared displacement. The above equation was applied to estimate free energy errors in all considered reactions, and the corresponding values are collected in Table 3. In most of the cases, the errors are in order of 2 kcal/mol (~3 k_BT), which is consistent with previous studies[39,40] where a similar computational scheme was applied.

Table 3. Summary of the Calculated Free-Energy Barriers (See Figures 2 and 3) along with Estimated Errors (in kcal/mol)

$\Delta F^{\#}$	$VO_2^+ \rightarrow VO^{2+}$	$VO^{2+} \rightarrow VO_2^+$
a	11.7 ± 2.3	14.6 ± 3.5
b	3.6 ± 1.5	9.6 ± 1.3
c	5.2 ± 1.9	11.7 ± 1.9
d		14.0 ± 2.0

4. CONCLUSIONS

In summary, we have performed a detailed CPMD-based metadynamics investigation of the VO_2^+/VO^{2+} redox reaction mechanism at the graphite edge/water interface relevant to all-VRFBs. By focusing on the graphite $(11\bar{2}0)$ edge surface functionalized by surface C═O groups as a representative carbon electrode material, we have analyzed the kinetics of $VO_2^+ \leftrightarrow VO^{2+}$ transformations at the interface and compared it with the results previously obtained for the V^{2+}/V^{3+} couple.

Our simulations reveal the catalytic role of surface oxygen groups in transferring an electron to the monodentate-adsorbed vanadium species along the C−O−V bond with the charge transfer process being coupled to proton transfer between oxygen species of the vanadium ions and aqueous electrolyte species. It is determined that the VO_2^+/VO^{2+} redox reaction does not involve the transfer of an oxygen atom, which was hypothesized to limit the overall reaction as a slow ionic process. Instead, oxygen atoms of the V ions serve as a conduit for proton exchange reactions in acidic electrolyte, which are found to be spontaneous for the discharge and energy-intensive for the charge processes. Given relatively high adsorption/desorption activation barriers, our results suggest that chemisorption of the vanadium ions to the graphite surface to form inner-sphere complexes and desorption from the surface after ET should limit the overall redox reaction process for both V^{2+}/V^{3+} and VO_2^+/VO^{2+} redox couples, with V^{2+}/V^{3+} being the rate-determining step during the discharge process.

The identified mechanism does not rule out the possibility of formation of vanadium-oxide layer passivating the surface as our simulations correspond to the dilute regime of vanadium interaction with the graphite surface. At high vanadium concentrations, however, such surface passivation may become pronounced because of interactions between adsorbed vanadium species, thereby impeding the VO_2^+/VO^{2+} redox reaction as observed in some experiments. Moreover, our simulations reveal the formation of reaction intermediates at the interface, featuring OH groups in the first coordination sphere of V. Such intermediates are known to play a key role in condensation reactions that can lead to the formation of vanadium-oxide precipitates at graphite surfaces, which is in agreement with experimental observations for VO_2^+/VO^{2+}.

■ ASSOCIATED CONTENT

Supporting Information

The Supporting Information is available free of charge on the ACS Publications website at DOI: 10.1021/acsami.8b05864.

Example of NWChem input file (PDF)

Computational details and error analysis (PDF)

■ AUTHOR INFORMATION

Corresponding Author

*E-mail: valexandrov2@unl.edu. Phone: +1 402 4725323.

ORCID

Konstantin Klyukin: 0000-0001-8325-8725

Vitaly Alexandrov: 0000-0003-2063-6914

Notes

The authors declare no competing financial interest.

■ ACKNOWLEDGMENTS

This work used the Extreme Science and Engineering Discovery Environment (XSEDE),[48] which is supported by National Science Foundation grant number ACI-1548562, and the Holland Computing Center at the University of Nebraska−Lincoln. V.A. also gratefully acknowledges financial support from the startup package.

■ REFERENCES

(1) Weber, A. Z.; Mench, M. M.; Meyers, J. P.; Ross, P. N.; Gostick, J. T.; Liu, Q. Redox Flow Batteries: a Review. *J. Appl. Electrochem.* **2011**, *41*, 1137.

(2) Noack, J.; Roznyatovskaya, N.; Herr, T.; Fischer, P. The Chemistry of Redox-Flow Batteries. *Angew. Chem., Int. Ed.* **2015**, *54*, 9776−9809.

(3) Soloveichik, G. L. Flow Batteries: Current Status and Trends. *Chem. Rev.* **2015**, *115*, 11533−11558.

(4) Park, M.; Ryu, J.; Wang, W.; Cho, J. Material Design and Engineering of Next-Generation Flow-Battery Technologies. *Nat. Rev. Mater.* **2016**, *2*, 16080.

(5) Gong, K.; Xu, F.; Grunewald, J. B.; Ma, X.; Zhao, Y.; Gu, S.; Yan, Y. All-Soluble All-Iron Aqueous Redox-Flow Battery. *ACS Energy Lett.* **2016**, *1*, 89−93.

(6) Wei, X.; Pan, W.; Duan, W.; Hollas, A.; Yang, Z.; Li, B.; Nie, Z.; Liu, J.; Reed, D.; Wang, W.; Sprenkle, V. Materials and Systems for Organic Redox Flow Batteries: Status and Challenges. *ACS Energy Lett.* **2017**, *2*, 2187−2204.

(7) Kamat, P. V.; Schanze, K. S.; Buriak, J. M. Redox Flow Batteries. *ACS Energy Lett.* **2017**, *2*, 1368−1369.

(8) Zhong, S.; Skyllas-Kazacos, M. Electrochemical Behaviour of Vanadium (V)/Vanadium (IV) Redox Couple at Graphite Electrodes. *J. Power Sources* **1992**, *39*, 1−9.

DOI: 10.1021/acsami.8b05864
ACS Appl. Mater. Interfaces 2018, 10, 20621−20626

(9) Li, L.; Kim, S.; Wang, W.; Vijayakumar, M.; Nie, Z.; Chen, B.; Zhang, J.; Xia, G.; Hu, J.; Graff, G.; Liu, J.; Yang, Z. A Stable Vanadium Redox-Flow Battery with High Energy Density for Large-Scale Energy Storage. *Adv. Energy Mater.* **2011**, *1*, 394−400.
(10) Vijayakumar, M.; Li, L.; Graff, G.; Liu, J.; Zhang, H.; Yang, Z.; Hu, J. Z. Towards Understanding the Poor Thermal Stability of V5+ Electrolyte Solution in Vanadium Redox Flow Batteries. *J. Power Sources* **2011**, *196*, 3669−3672.
(11) Parasuraman, A.; Lim, T. M.; Menictas, C.; Skyllas-Kazacos, M. Review of Material Research and Development for Vanadium Redox Flow Battery Applications. *Electrochim. Acta* **2013**, *101*, 27−40.
(12) Vijayakumar, M.; Nie, Z.; Walter, E.; Hu, J.; Liu, J.; Sprenkle, V.; Wang, W. Understanding Aqueous Electrolyte Stability through Combined Computational and Magnetic Resonance Spectroscopy: A Case Study on Vanadium Redox Flow Battery Electrolytes. *ChemPhysChem* **2015**, *80*, 428−437.
(13) Kim, K. J.; Park, M.-S.; Kim, Y.-J.; Kim, J. H.; Dou, S. X.; Skyllas-Kazacos, M. A Technology Review of Electrodes and Reaction Mechanisms in Vanadium Redox Flow Batteries. *J. Mater. Chem. A* **2015**, *3*, 16913−16933.
(14) Park, M.; Ryu, J.; Cho, J. Nanostructured Electrocatalysts for All-Vanadium Redox Flow Batteries. *Chem.—Asian J.* **2015**, *10*, 2096−2110.
(15) Sun, B.; Skyllas-Kazacos, M. Modification of Graphite Electrode Materials for Vanadium Redox Flow Battery Application-I. Thermal Treatment. *Electrochim. Acta* **1992**, *37*, 1253−1260.
(16) Wang, W. H.; Wang, X. D. Investigation of Ir-Modified Carbon Felt as the Positive Electrode of an all-Vanadium Redox Flow Battery. *Electrochim. Acta* **2007**, *52*, 6755−6762.
(17) Zhou, H.; Shen, Y.; Xi, J.; Qiu, X.; Chen, L. ZrO2-Nanoparticle-Modified Graphite Felt: Bifunctional Effects on Vanadium Flow Batteries. *ACS Appl. Mater. Interfaces* **2016**, *8*, 15369−15378.
(18) Huang, P.; Ling, W.; Sheng, H.; Zhou, Y.; Wu, X.; Zeng, X.-X.; Wu, X.; Guo, Y.-G. Heteroatom-Doped Electrodes for All-Vanadium Redox Flow Batteries with Ultralong Lifespan. *J. Mater. Chem. A* **2018**, *6*, 41−44.
(19) Fink, H.; Friedl, J.; Stimming, U. Composition of the Electrode Determines Which Half-Cell's Rate Constant is Higher in a Vanadium Flow Battery. *J. Phys. Chem. C* **2016**, *120*, 15893−15901.
(20) Liu, T.; Li, X.; Xu, C.; Zhang, H. Activated Carbon Fiber Paper Based Electrodes with High Electrocatalytic Activity for Vanadium Flow Batteries with Improved Power Density. *ACS Appl. Mater. Interfaces* **2017**, *9*, 4626−4633.
(21) Pour, N.; Kwabi, D. G.; Carney, T.; Darling, R. M.; Perry, M. L.; Shao-Horn, Y. Influence of Edge-and Basal-Plane Sites on the Vanadium Redox Kinetics for Flow Batteries. *J. Phys. Chem. C* **2015**, *119*, 5311−5318.
(22) Estevez, L.; Reed, D.; Nie, Z.; Schwarz, A. M.; Nandasiri, M. I.; Kizewski, J. P.; Wang, W.; Thomsen, E.; Liu, J.; Zhang, J.-G.; Sprenkle, V.; Li, B. Tunable Oxygen Functional Groups as Electrocatalysts on Graphite Felt Surfaces for All-Vanadium Flow Batteries. *ChemSusChem* **2016**, *9*, 1455−1461.
(23) Aaron, D.; Sun, C.-N.; Bright, M.; Papandrew, A. B.; Mench, M. M.; Zawodzinski, T. A. In Situ Kinetics Studies in All-Vanadium Redox Flow Batteries. *ECS Electrochem. Lett.* **2013**, *2*, A29−A31.
(24) Jiang, Z.; Klyukin, K.; Alexandrov, V. First-principles Study of Adsorption-Desorption Kinetics of Aqueous V2+/V3+ Redox Species on Graphite in a Vanadium Redox Flow Battery. *Phys. Chem. Chem. Phys.* **2017**, *19*, 14897−14901.
(25) Friedl, J.; Bauer, C. M.; Rinaldi, A.; Stimming, U. Electron Transfer Kinetics of the VO2+/VO+2 - Reaction on Multi-walled Carbon Nanotubes. *Carbon* **2013**, *63*, 228−239.
(26) Valiev, M.; Bylaska, E. J.; Govind, N.; Kowalski, K.; Straatsma, T. P.; Van Dam, H. J. J.; Wang, D.; Nieplocha, J.; Apra, E.; Windus, T. L.; de Jong, W. A. NWChem: a Comprehensive and Scalable Open-Source Solution for Large Scale Molecular Simulations. *Comput. Phys. Commun.* **2010**, *181*, 1477−1489.
(27) Perdew, J. P.; Burke, K.; Ernzerhof, M. Generalized Gradient Approximation Made Simple. *Phys. Rev. Lett.* **1996**, *77*, 3865.
(28) Grimme, S.; Ehrlich, S.; Goerigk, L. Effect of the Damping Function in Dispersion Corrected Density Functional Theory. *J. Comput. Chem.* **2011**, *32*, 1456−1465.
(29) Troullier, N.; Martins, J. L. Efficient Pseudopotentials for Plane-Wave Calculations. *Phys. Rev. B: Condens. Matter Mater. Phys.* **1991**, *43*, 1993.
(30) Hamann, D. R.; Schlüter, M.; Chiang, C. Norm-Conserving Pseudopotentials. *Phys. Rev. Lett.* **1979**, *43*, 1494.
(31) Hamann, D. R. Generalized Norm-Conserving Pseudopotentials. *Phys. Rev. B: Condens. Matter Mater. Phys.* **1989**, *40*, 2980.
(32) Jiang, Z.; Klyukin, K.; Alexandrov, V. Structure, Hydrolysis, and Diffusion of Aqueous Vanadium Ions from Car-Parrinello Molecular Dynamics. *J. Chem. Phys.* **2016**, *145*, 114303.
(33) Bon, M.; Laino, T.; Curioni, A.; Parrinello, M. Characterization of Vanadium Species in Mixed Chloride−Sulfate Solutions: An Ab Initio Metadynamics Study. *J. Phys. Chem. C* **2016**, *120*, 10791−10798.
(34) Nibel, O.; Bon, M.; Agiorgousis, M. L.; Laino, T.; Gubler, L.; Schmidt, T. J. Unraveling the Interaction Mechanism between Amidoxime Groups and Vanadium Ions at Various pH Conditions. *J. Phys. Chem. C* **2017**, *121*, 6436−6445.
(35) Intan, N. N.; Klyukin, K.; Zimudzi, T. J.; Hickner, M. A.; Alexandrov, V. A Combined Theoretical-Experimental Study of Interactions between Vanadium Ions and Nafion Membrane in All-Vanadium Redox Flow Batteries. *J. Power Sources* **2018**, *373*, 150−160.
(36) Car, R.; Parrinello, M. Unified Approach for Molecular Dynamics and Density-Functional Theory. *Phys. Rev. Lett.* **1985**, *55*, 2471.
(37) Bussi, G.; Laio, A.; Parrinello, M. Equilibrium Free Energies from Nonequilibrium Metadynamics. *Phys. Rev. Lett.* **2006**, *96*, 090601.
(38) Laio, A.; Gervasio, F. L. Metadynamics: a Method to Simulate Rare Events and Reconstruct the Free Energy in Biophysics, Chemistry and Material Science. *Rep. Prog. Phys.* **2008**, *71*, 126601.
(39) Stirling, A.; Pápai, I. H2CO3 Forms via HCO−3 in Water. *J. Phys. Chem. B* **2010**, *114*, 16854−16859.
(40) Stirling, A. HCO−3-Formation from CO2 at High pH: Ab Initio Molecular Dynamics Study. *J. Phys. Chem. B* **2011**, *115*, 14683−14687.
(41) Cheng, T.; Xiao, H.; Goddard, W. A., III Reaction mechanisms for the electrochemical reduction of CO2 to CO and formate on the Cu (100) surface at 298 K from quantum mechanics free energy calculations with explicit water. *J. Am. Chem. Soc.* **2016**, *138*, 13802−13805.
(42) Klyukin, K.; Alexandrov, V. CO2 Adsorption and Reactivity on Rutile TiO2 (110) in Water: An Ab Initio Molecular Dynamics Study. *J. Phys. Chem. C* **2017**, *121*, 10476−10483.
(43) Nosé, S. A Molecular Dynamics Method for Simulations in the Canonical Ensemble. *Mol. Phys.* **1984**, *52*, 255−268.
(44) Hoover, W. G. Canonical Dynamics: Equilibrium Phase-Space Distributions. *Phys. Rev. A: At., Mol., Opt. Phys.* **1985**, *31*, 1695.
(45) Cauët, E.; Bogatko, S.; Weare, J. H.; Fulton, J. L.; Schenter, G. K.; Bylaska, E. J. Structure and Dynamics of the Hydration Shells of the Zn2+ Ion from ab Initio Molecular Dynamics and Combined ab Initio and Classical Molecular Dynamics Simulations. *J. Chem. Phys.* **2010**, *132*, 194502.
(46) Xu, M.; Xiao, P.; Stauffer, S.; Song, J.; Henkelman, G.; Goodenough, J. B. Theoretical and Experimental Study of Vanadium-Based Fluorophosphate Cathodes for Rechargeable Batteries. *Chem. Mater.* **2014**, *26*, 3089−3097.
(47) Leung, K. First-Principles Modeling of Mn(II) Migration above and Dissolution from Li_xMn2O4 (001) Surfaces. *Chem. Mater.* **2017**, *29*, 2550−2562.
(48) Towns, J.; Cockerill, T.; Dahan, M.; Foster, I.; Gaither, K.; Grimshaw, A.; Hazlewood, V.; Lathrop, S.; Lifka, D.; Peterson, G. D.; Roskies, R.; Scott, J. R.; Wilkens-Diehr, N. XSEDE: Accelerating Scientific Discovery. *Comput. Sci. Eng.* **2014**, *16*, 62−74.

DOI: 10.1021/acsami.8b05864
ACS Appl. Mater. Interfaces 2018, 10, 20621−20626